LA-12623-MS

UC-907
Issued: January 1994

BOMAB Phantom Manufacturing Quality Assurance Study Using Monte Carlo Computations

Michael W. Mallett

Los Alamos
NATIONAL LABORATORY
Los Alamos, New Mexico 87545

BOMAB PHANTOM MANUFACTURING QUALITY ASSURANCE STUDY USING MONTE CARLO COMPUTATIONS

by

Michael W. Mallett

ABSTRACT

Monte Carlo calculations have been performed to assess the importance of and quantify quality assurance protocols in the manufacturing of the Bottle-Manikin-Absorption (BOMAB) phantom for calibrating in vivo measurement systems. The parameters characterizing the BOMAB phantom that were examined included height, fill volume, fill material density, wall thickness, and source concentration. Transport simulation was performed for monoenergetic photon sources of 0.200, 0.662, and 1.460 MeV. A linear response was observed in the photon current exiting the exterior surface of the BOMAB phantom due to variations in these parameters. Sensitivity studies were also performed for an in vivo system in operation at the Pacific Northwest Laboratories in Richland, WA. Variations in detector current for this in vivo system are reported for changes in the BOMAB phantom parameters studied here. Physical justifications for the observed results are also discussed.

I. INTRODUCTION

A study is currently being performed to assess the importance of quality assurance protocols in the manufacturing of the Bottle-Manikin-Absorption (BOMAB) phantom for calibrating in vivo measurement systems. The BOMAB phantom is a surrogate human structure used to calibrate an in vivo measurement system specifically for a whole body distribution of radioactivity. The phantom consists of ten hollow bottles which are right

circular cylinders or right elliptical cylinders in shape, each representing a different section of the human body as shown in Fig. 1. The walls are constructed of 4.76-mm-thick high-density polyethylene, and may be filled with appropriate tissue substitute materials. The dimensions of the standard BOMAB phantom representing the average adult male human body are given in Table 1.

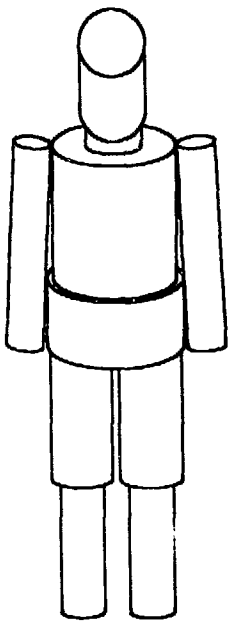

Fig. 1. The Bottle-Manikin-Absorption (BOMAB) Phantom.

Table 1. Standard BOMAB Phantom Dimensions for the Average Adult Male Human Body.

Bottle/body section	Cylinder shape	Cross section (cm)	Vertical height (cm)	Fill volume (cm^3)
Head	Right elliptical	19 x 14	20	3523
Neck	Right circular	13	10	1032
Thorax	Right elliptical	30 x 20	40	16,969
Pelvis	Right elliptical	36 x 20	20	9987
Thigh (2)	Right circular	15	40	6052 (ea)
Leg (2)	Right circular	12	40	3743 (ea)
Arm (2)	Right circular	10	60	3797 (ea)

All walls are composed of 4.76-mm-thick high-density polyethylene.

The study is being conducted by utilizing Monte Carlo methods to sample photon fields emanating from radioactive sources distributed among the ten BOMAB phantom bottles. The general-purpose Monte Carlo code MCNP, Version 4, developed at the Los Alamos National Laboratory (LANL) is used to perform the computations (Briesmeister and Hendricks 1991). The development of the method for performing radiation transport computations using MCNP with regard to the BOMAB phantom has been given previously (Mallett 1993a). Further modifications to the MCNP code itself have been

made to better facilitate Monte Carlo computations utilizing the BOMAB phantom design, in addition to improving the detail of the geometry model and accuracy of the sampling techniques used (Mallett 1993b). The purpose of this paper is to publish a portion of the results of this study rather than to describe the modified MCNP code. Hence, the literature should be consulted for specific details regarding development and implementation of the revised code.

This study involves varying the parameters that characterize the BOMAB phantom and then observing the resulting change in photon current at the exterior surface of the phantom. A study of the sensitivity of particular in vivo measurement systems to changes in the characteristic BOMAB parameters is also being performed. The objective of this facet of the study is to better understand and assess the applicability of the standard BOMAB phantom towards supplying generic system calibration efficiencies for the entire measurement population at a given facility. Those in vivo measurement systems included in the study are located at LANL, the Sandia National Laboratories (SNL) in Albuquerque, NM, and the Pacific Northwest Laboratories (PNL) in Richland, WA. Each facility represents a different detector system design in the measurement of whole body distributed radionuclides. This report contains the Monte Carlo results for the PNL in vivo measurement system only. The Monte Carlo results estimating the BOMAB phantom exterior surface current are also presented.

The PNL in vivo measurement system consists of five NaI scintillation detectors as shown in Fig. 2. Four of these detectors are 24 cm in diameter; one is 29 cm in diameter. Each crystal is 10 cm thick. The detector system is located posterior to the upright subject during the measurement. The detectors are mounted such that the face of each is tangent to a common plane 2.5 cm from the posterior surface of the subject, in this case the BOMAB phantom. In addition, a 1.3-cm-thick Plexiglas plate is located in the space

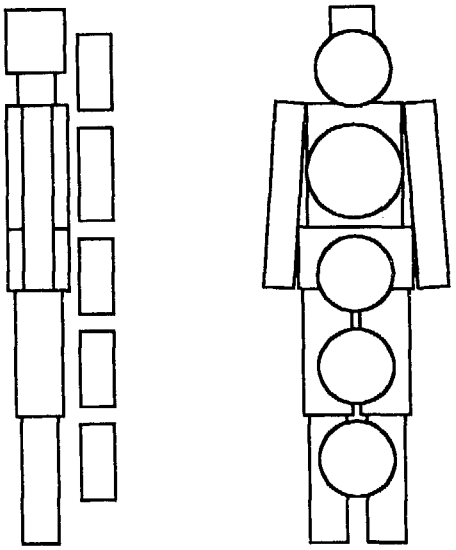

Fig. 2. The BOMAB phantom positioned for calibration of the five-NaI-detector in vivo system currently operated at PNL. The phantom is configured in the "centerline" geometry (i.e., a common axis or plane passes through the center of each bottle in the vertical direction). Four of the detectors are 24 cm in diameter; one is 29 cm in diameter. Each detector is 10 cm in thickness.

between the subject and the detectors. The BOMAB phantom was configured in the "centerline" geometry (i.e., positioned along a central axis common to all bottles) for calibration of the PNL detector system as shown in Fig. 2.

II. DESCRIPTION OF EXPERIMENTS

The change in photon current at the exterior surface of the BOMAB phantom and the subsequent variation in detector current for the in vivo measurement systems studied here were observed by varying parameters characterizing the structure of the phantom. Each experiment discussed below describes the parameter of interest and the degree to which it was varied, as well as additional constraints regarding the BOMAB structure that were imposed for each test. The notation used to define characteristic parameters is

shown in Fig. 3, including the standard dimension and the modified value. The notation includes the following:

a: one-half the axis in the defined $\hat{x}$ direction,

b: one-half the axis in the defined $\hat{y}$ direction,

z: height in the defined $\hat{z}$ direction,

t: wall thickness,

' denotes inner dimension, and

* denotes modified dimension.

The modified values of these and other pertinent parameters for each experiment are listed in Appendix A.

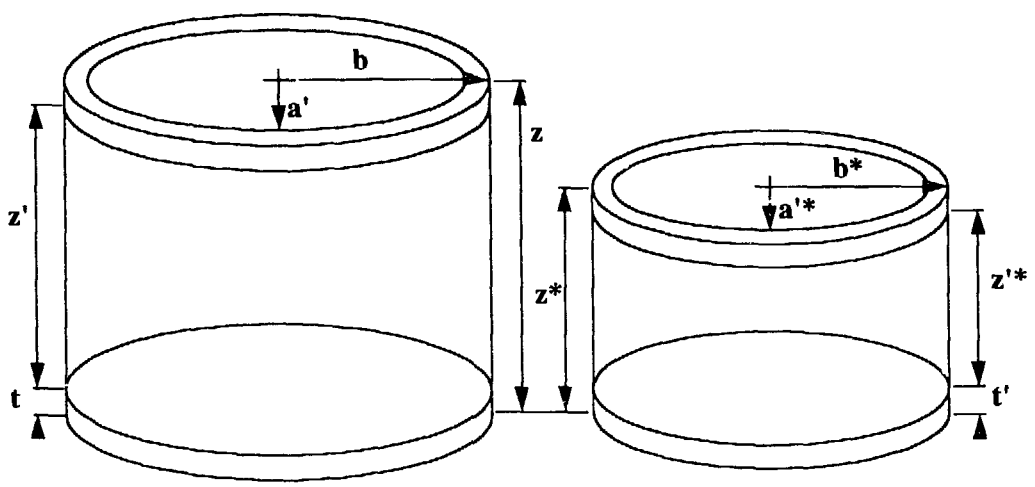

Fig. 3. Diagram of notation used to describe the BOMAB phantom characteristic parameters: **a**, **b**, and **z** refer to measurements in the defined $\hat{x}$-, $\hat{y}$-, and $\hat{z}$-axis directions, respectively. Other notations include the following: **t** denotes wall thickness, ' refers to inner dimensions, and * refers to a modified dimension different from the value listed in Table 1.

Experiment #1. Vary the height.

The height (z) of each bottle was varied by ±5%, ±10%, and ±20%. In each case, the fill volume of the bottle, given by:

$$\text{Fill Volume} = a'^* \times b'^* \times z'^* \times \pi, \quad (1)$$

was held constant (see Fig. 3). In order to hold the fill volume constant, an additional restraint was required:

$$\frac{a'}{a'^*} = \frac{b'}{b'^*}. \quad (2)$$

Experiment #2. Vary the fill volume.

The fill volume given in Eq. (1) was varied by ±5%, ±10%, and ±20%. This was performed by two methods:

Experiment #2A required holding the height of each bottle constant while varying the parameters defining the fill volume according to Eq. (2).

Experiment #2B permitted the height of each bottle to change such that

$$\frac{a'}{a'^*} = \frac{b'}{b'^*} = \frac{z'}{z'^*}. \quad (3)$$

Experiment #3. Vary the density of the fill material.

The density of the fill material was varied by ±5%, ±10%, and ±20%. This was performed by varying the density of two fill materials, specifically polyurethane and water.

Experiment #3A used polyurethane, standard density ρ=1.09 g cm^{-3}, as the fill material.

Experiment #3B used water, standard density ρ=1.00 g cm^{-3}, as the fill material.

Experiment #4. Vary the wall thickness.

The walls of each standard phantom bottle are composed of 4.76-mm-thick high-density polyethylene (ρ=0.95 g cm^{-3}). The wall thickness was varied by ±5%, ±10%, and ±20%, as well as increased to 10 mm. The fill volume was held constant in each case.

Experiment #5. Vary the source concentration of the fill material.

The source concentration of the fill material was varied by ±5%, ±10%, and ±20%. This was performed by three methods:

Experiment #5A varied the source concentration of the thorax bottle.

Experiment #5B varied the source concentration of the pelvis bottle.

Experiment #5C varied the source concentration of the thorax, pelvis, and arm bottles proportionately.

In each case, polyurethane (ρ=1.09 g cm^{-3}) was used as the fill material (Griffith *et al.* 1978).

III. DATA REPORTING

The Monte Carlo computation results using the modified MCNP code for each experiment described above are tabulated in Appendix B and displayed graphically in Appendix C. The results for Experiment #1 are also reported in Table 2 and are shown graphically in Figs. 4-6 to facilitate interpretation of the reporting protocol and photon sampling techniques used by the code. Recall, Experiment #1 varied the height of each bottle while holding the fill volume constant.

The Monte Carlo computations were performed individually for source photons having an energy of 0.200, 0.662, and 1.460 MeV. The source photons were distributed uniformly throughout the total fill volume of the phantom, except as specified in Experiments #5A-C. Hence, the source concentration (source particles cm^{-3}) was identical within each bottle. The data plotted in Fig. 4 are the Monte Carlo results of sampling source energy photons crossing the exterior surface of the BOMAB phantom, normalized per source photon (i.e., the relative surface current.) The exterior surface of the BOMAB phantom is defined as the total surface area of the phantom bottles not overlapped by adjacent bottles. For example, the neck bottle has two end surfaces completely overlapped by the end surfaces of the adjacent head and thorax bottles. Hence, the neck bottle contribution to the total exterior surface area of the phantom

Table 2. Monte Carlo Results for Different Phantom Heights (Experiment #1).

Relative BOMAB surface current
(source energy photons/source photon)

% change	200 keV	3σ	662 keV	3σ	1460 keV	3σ
-20%	0.331710	0.004478	0.453070	0.004757	0.557120	0.004680
-10%	0.342120	0.004516	0.464040	0.004733	0.567740	0.004769
-5%	0.347160	0.004478	0.469450	0.004788	0.572730	0.004639
0%	0.352097	0.001479	0.473819	0.001564	0.577123	0.001558
5%	0.357260	0.004501	0.479270	0.004745	0.582470	0.004718
10%	0.361840	0.004559	0.484300	0.004795	0.587490	0.004582
20%	0.370410	0.004556	0.493160	0.004734	0.596460	0.004652

Relative PNL in vivo system detector current
(source energy photons incident upon detectors/source photon)

% change	200 keV	3σ	662 keV	3σ	1460 keV	3σ
-20%	0.043379	0.000612	0.060375	0.000706	0.075330	0.000791
-10%	0.047599	0.000643	0.065636	0.000748	0.081459	0.000831
-5%	0.047973	0.000648	0.065900	0.000751	0.081506	0.000831
0%	0.048046	0.000202	0.065956	0.000237	0.081499	0.000269
5%	0.048361	0.000638	0.066000	0.000752	0.081492	0.000831
10%	0.048355	0.000638	0.065939	0.000752	0.081114	0.000827
20%	0.046934	0.000634	0.063681	0.000726	0.077889	0.000794

Relative PNL 29-cm NaI detector current
(source energy photons incident upon 29-cm NaI detector/source photon)

% change	200 keV	3σ	662 keV	3σ	1460 keV	3σ
-20%	0.013213	0.000341	0.018628	0.000408	0.023501	0.000451
-10%	0.016134	0.000378	0.022721	0.000450	0.028653	0.000499
-5%	0.016549	0.000382	0.023253	0.000453	0.029302	0.000510
0%	0.016479	0.000119	0.023265	0.000140	0.029343	0.000158
5%	0.016490	0.000381	0.023082	0.000450	0.029140	0.000507
10%	0.016247	0.000380	0.022818	0.000445	0.028652	0.000499
20%	0.015639	0.000371	0.021919	0.000441	0.027361	0.000492

consists strictly of the side surface area (i.e., the circumference times the height.) Additionally, the exterior surface areas of the two adjacent bottles are reduced by the surface area equal to the end surfaces of the neck bottle.

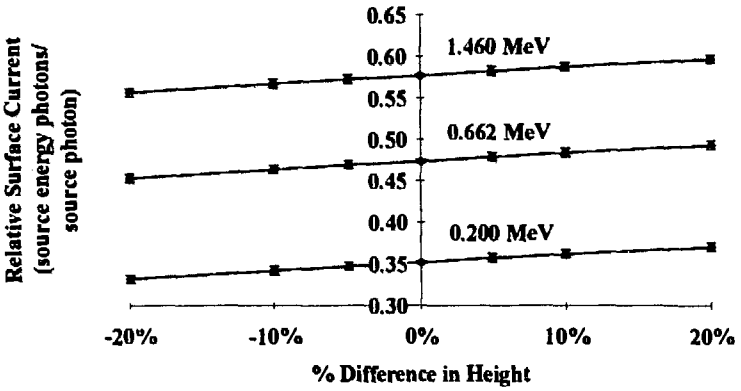

Fig. 4. Relative BOMAB surface current Monte Carlo results for different phantom heights (Experiment #1). Errors shown are ±3σ.

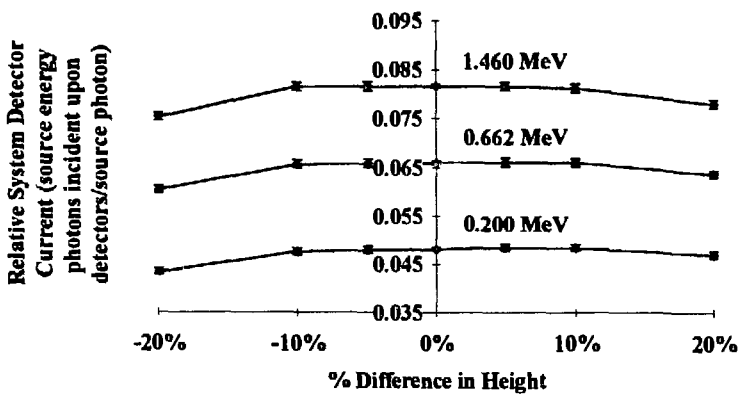

Fig. 5. Relative PNL in vivo system detector current Monte Carlo results for different phantom heights (Experiment #1). Errors shown are ±3σ.

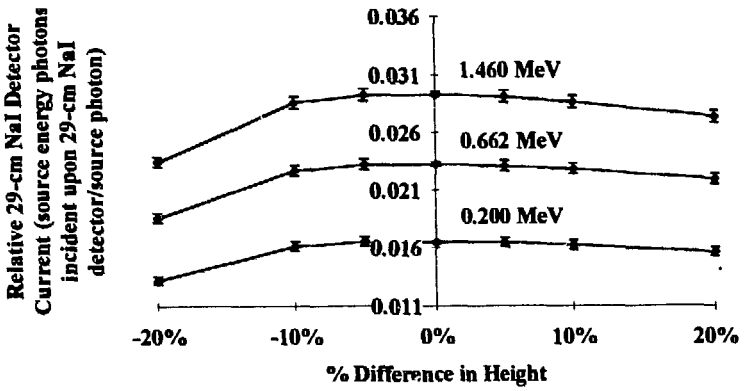

Fig. 6. Relative PNL 29-cm NaI detector current Monte Carlo results for different phantom heights (Experiment #1). Errors shown are $\pm 3\sigma$.

The Monte Carlo results of Fig. 4 were estimated by tallying photons using a 2 keV-wide energy bin below the source energy. For example, a photon having a source energy of 0.200 MeV was tallied at the exterior surface of the phantom if it emerged with an energy between 0.198 and 0.200 MeV. Each data point for the experiment was determined by processing 100,000 source photons. However, the data points for 0% change in height (i.e., 0% change in all parameters) represent the Monte Carlo results for the standard BOMAB phantom of the dimensions given in Table 1, and were determined by sampling 1,000,000 source photons. The error reported for each data point is $\pm 3\sigma$ based on the relative error estimated by MCNP. Results are for the centerline geometry configuration as previously noted.

The results shown in Figs. 5 and 6 are specific to the PNL in vivo measurement system described above. The data plotted in Fig. 5 are the Monte Carlo results of sampling source energy photons incident upon one of the five detectors. The Monte Carlo results are normalized per source photon, and thus represent the relative detector current for the in vivo system. The tallies were compiled using a 2 keV-wide energy bin below the source energy. Figure 6 displays the Monte Carlo results solely for the 29-cm NaI

detector. Each data point for the experiment was determined by processing 1,000,000 source photons. The data points for the standard BOMAB phantom dimensions (i.e., 0% change) were determined by sampling 10,000,000 source photons. The error reported for each data point is $\pm 3\sigma$ based on the relative error estimated by MCNP. Results are for the centerline geometry configuration as previously noted.

The data displayed in Figs. 5 and 6 should not be confused with the absolute detection efficiency of the system. The Monte Carlo results presented here must be corrected by an appropriately determined intrinsic efficiency (counts per γ incident) for each detector in order to determine the absolute detection efficiency of the system (Mallett 1993c). However, the Monte Carlo results represent a means by which to compare changes in the relative sensitivity of the in vivo measurement system for a given variation in the BOMAB parameters. This comparison requires making the reasonable assumption that the intrinsic efficiency of each detector is unaffected by the changes in the BOMAB phantom construction studied here.

IV. DISCUSSION

The Monte Carlo results presented in Appendices B and C reflect physical aspects of the calibration process that warrant discussion. First, the photon current for the exterior surface of the BOMAB phantom is shown to be a linear function of the percentage difference in each of the sensitivity studies performed here. This fact is evident in Fig. 4 for Experiment #1 in which the height of the phantom was varied. In this instance, the linear response may be easily understood by considering the change in surface area (S) relative the volume (V) for each bottle. It has been shown that the mean chord length (L) for a convex volume is equal to 4V/S (ICRU 1980). Table 3 reports the exterior surface area, the fill volume (held constant), and the mean chord length of each

bottle as a function of the change in the height of the phantom for Experiment #1. Note that a slight error has been introduced due to the calculation of the mean chord length using the exterior surface area rather than the surface of the fill volume. However, the following results show this error to be insignificant in relating changes in the calculated mean chord length to changes in the surface current.

The variation in the mean chord length for the entire BOMAB phantom at each percentage change in height is of interest. However, it is the attenuation of the source photons for the given mean chord length of each bottle that must be considered. The effective mean chord length for the entire BOMAB phantom, L_{eff}, may be calculated by exponentially averaging the mean chord length in each bottle, as given by

$$L_{eff} = \left(\frac{-1}{\mu_{E_\gamma}} \right) \times \ln \left[\sum \exp\left(-\mu_{E_\gamma} \times L_i \right) \right], \qquad (4)$$

where μ_{E_γ} is the linear attenuation coefficient for polyurethane at E_γ (ICRU 1989). Table 3 reports the effective mean chord length for each change in the height of the phantom at each photon energy studied here. Similarly, the effective mean attenuation by the phantom is given by

$$\text{effective mean attenuation} = \sum \exp\left(-\mu_{E_\gamma} \times L_i \right). \qquad (5)$$

The effective mean attenuation is reported in Table 3 and is also displayed graphically in Fig. 7. The linear change in the effective mean attenuation that is evident in Fig. 7 can be inferred as the physical justification for the linear change in the BOMAB surface current observed in Fig. 4. Similar findings are true for the remaining experiments in which either L_{eff} or μ_{E_γ} was varied.

Table 3. Experiment #1 Physical Parameters Defining Mean Attenuation.

Bottle	Exterior surface area (cm) -20%	-10%	-5%	0%	5%	10%	20%	Volume (cm^3)
head	1292.4	1310.4	1321.5	1333.7	1346.7	1360.4	1389.4	3523.0
neck	367.0	388.1	398.4	408.4	418.3	428.0	446.9	1031.5
thorax	3283.0	3412.5	3477.5	3542.3	3607.0	3671.3	3798.8	16968.9
pelvis	2034.9	2082.3	2108.6	2136.0	2164.3	2193.3	2252.8	9987.4
thigh (ea)	1758.9	1855.3	1902.3	1948.6	1994.1	2038.9	2126.6	6052.3
leg (ea)	1481.1	1551.5	1586.4	1621.1	1655.4	1689.5	1756.6	3743.3
arm (ea)	1865.2	1954.1	1998.2	2042.0	2085.6	2128.8	2214.1	3796.6

Bottle	Mean chord length (cm) -20%	-10%	-5%	0%	5%	10%	20%
head	10.9	10.8	10.7	10.6	10.5	10.4	10.1
neck	11.2	10.6	10.4	10.1	9.9	9.6	9.2
thorax	20.7	19.9	19.5	19.2	18.8	18.5	17.9
pelvis	19.6	19.2	18.9	18.7	18.5	18.2	17.7
thigh (ea)	13.8	13.0	12.7	12.4	12.1	11.9	11.4
leg (ea)	10.1	9.7	9.4	9.2	9.0	8.9	8.5
arm (ea)	8.1	7.8	7.6	7.4	7.3	7.1	6.9

Energy (MeV)	Effective mean chord length (cm) -20%	-10%	-5%	0%	5%	10%	20%	μ/ρ ($cm^2\ g^{-1}$)
0.200	11.60	11.14	10.93	10.72	10.53	10.34	9.99	0.134
0.667	11.94	11.46	11.24	11.03	10.82	10.63	10.27	0.0845
1.460	12.15	11.66	11.43	11.22	11.01	10.81	10.44	0.0574

Energy (MeV)	Effective mean attenuation (unattenuated source energy photons/source photon) -20%	-10%	-5%	0%	5%	10%	20%
0.200	0.1836	0.1964	0.2026	0.2088	0.2149	0.2209	0.2325
0.667	0.3330	0.3479	0.3551	0.3621	0.3690	0.3757	0.3885
1.460	0.4677	0.4821	0.4890	0.4957	0.5022	0.5085	0.5205

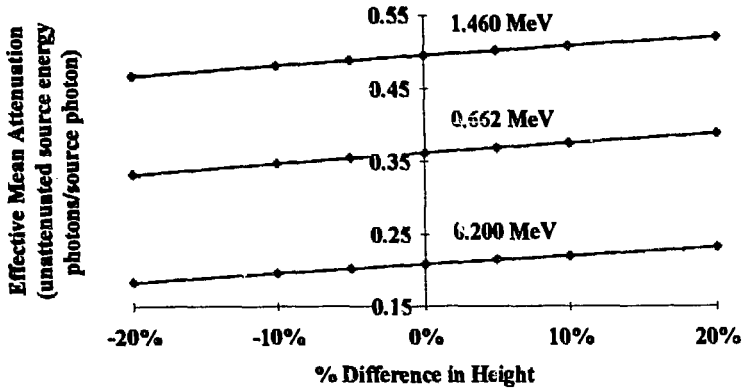

Fig. 7. Effective mean attenuation by the BOMAB phantom for different phantom heights (Experiment #1).

Monte Carlo results specific to the PNL in vivo measurement system are included in Appendices B and C. The results of Experiment #1 for the entire system as well as for the 29-cm NaI detector only are shown graphically in Figs. 5 and 6, respectively. The data shown in Fig. 5 indicate that the sensitivity of the PNL system is relatively independent of changes in height except at relatively extreme values (i.e., ±20%). That is, variations in the phantom height by ±10% (i.e., ranging in height from 153 - 187 cm) result in no detectable change in the sensitivity of the PNL in vivo system. Similarly, the data shown in Fig. 6 reflect the relatively stable detector current of the 29-cm NaI detector except at extreme heights.

Figures 5 and 6 show that the 29-cm NaI detector is responsible for ~35% of the PNL in vivo system detector current for this geometry. Hence, this study demonstrates the capability of using these Monte Carlo computations to assess the appropriate position of the 29-cm NaI detector in the PNL in vivo system with respect to variations in the height of subjects. Similar data for each detector and for a variety of phantom (or subject) characteristics could therefore be used to optimize the entire in vivo system design.

Monte Carlo results for the remaining experiments specific to the PNL in vivo system and the 29-cm NaI detector alone are included in Appendices B and C of this report. Changes in the source concentration of particular bottles (i.e., thorax, pelvis, and arms) performed in Experiments #5A-C indicate little variation in the overall system sensitivity. However, the relative detector current of the 29-cm NaI detector is obviously dependent upon the distribution of the source, and is particularly sensitive to variations in the source concentration of the thorax bottle (see Appendices B and C). This is to be expected given the position of the 29-cm NaI detector relative to the bottles with varied concentrations investigated here. The results for Experiments #2-4 show a significant relationship between the PNL in vivo system sensitivity and the particular BOMAB parameter considered in each case. This dependence can be attributed to a more significant change in self-absorption (i.e., dependence on L_{eff}) for a given percentage change in the BOMAB parameter, as compared with an identical percentage change in the height of the phantom (Experiment #1.) Also, the effective distance between the photon source origin and the detectors varies more for a given percentage change in the BOMAB parameters studied in Experiments #2-4 than for the same percentage change in the height of the phantom.

V. CONCLUSIONS

The Monte Carlo code MCNP, modified for directly handling the BOMAB phantom, was used to examine the importance of quality assurance protocols in the manufacturing of the BOMAB phantom with applicability to calibrating in vivo measurement systems. Sensitivity studies indicated a linear dependence of the photon current exiting the BOMAB phantom exterior surface as a function of those parameters characterizing the phantom studied here, specifically, height, fill volume, fill material density, wall thickness, and source concentration. Hence, quality assurance protocols in

the production of the BOMAB phantom are essential to ensuring consistent (or at least acceptable) standard photon fields emanating from the surface of mass-produced phantoms. The determination of appropriate quality controls can therefore be based on the linear response of the photon fields to variations in these BOMAB parameters.

The sensitivity studies also showed the dependence of the PNL in vivo system on variations in the phantom parameters. Changes in the sensitivity of the system were not observed to be linear in all cases. Hence, quality assurance protocols must be determined based on the specific in vivo system design considered. Towards this end, the Monte Carlo methods utilized here are useful in assessing the relative changes in the sensitivity of the system to given changes in the BOMAB phantom design. Similarly, this technique is an excellent means for determining the appropriateness of applying calibration efficiencies produced using the standard BOMAB phantom to the entire population at a given facility. For example, the standard BOMAB phantom-determined calibration efficiency for the PNL system is applicable to all subjects differing only in height within the range 153 - 187 cm. However, this calibration efficiency should not be applied to subjects well outside this height range. Similar conclusions regarding varying other BOMAB parameters must likewise be considered relative to the particular in vivo system design.

ACKNOWLEDGMENTS

PNL in vivo measurement system data were provided by Timothy P. Lynch, PNL. This manuscript was graciously reviewed by Robert W. Keys III and Hsiao-Hua Hsu of Health Physics Measurements, HS-4, and by Ileana Buican, Writing and Editing, IS-1, Los Alamos National Laboratory.

REFERENCES

Briesmeister, J. F.; Hendricks, J. S. MCNP4 Newsletter. Los Alamos, NM: Los Alamos National Laboratory; X-6:JFB-91-177; 1991.

Griffith, R. V.; Dean, P. N.; Anderson, A. L.; Fisher, J. C. Fabrication of a Tissue-Equivalent Torso Phantom for Intercalibration of In-Vivo Transuranic-Nuclide Counting Facilities. Livermore, CA: Lawrence Livermore Laboratory; UCRL-80343; 1978.

International Commission on Radiation Units and Measurements. Radiation Quantities and Units. Washington, D.C.: ICRU; ICRU Report 33; 1980.

International Commission on Radiation Units and Measurements. Tissue Substitutes in Radiation Dosimetry and Measurement. Bethesda, MD: ICRU; ICRU Report 44; 1989.

Mallett, M. W. In Vivo Measurement System Calibration Using Magnetic Resonance Imaging and Monte Carlo Computations. College Station, TX: Texas A&M University; 1993a. Ph.D. Dissertation.

Mallett, M. W. Calibration of In Vivo Measurement Systems with the BOMAB Phantom Using Monte Carlo Computations. Los Alamos, NM: Los Alamos National Laboratory; LA-UR-93-4256; 1993b.

Mallett, M. W. A Three-Point Method for Absolutely Determining the Intrinsic Efficiency of a Photon Detector Using Monte Carlo Computations. Los Alamos, NM: Los Alamos National Laboratory; LA-UR-93-3896; 1993c.

Experiment #1
Vary the height of the phantom.

% difference in height = -20%

bottle	a	a'	a*	b	b'	b*	z	z'	z*	t
head	9.5	9.024	10.629	7.0	6.524	7.816	20.0	19.048	16.000	0.476
neck	6.5	6.024	7.301	6.5	6.024	7.301	10.0	9.048	8.000	0.476
thorax	10.0	9.524	11.157	15.0	14.524	16.764	40.0	39.048	32.000	0.476
pelvis	10.0	9.524	11.191	18.0	17.524	20.192	20.0	19.048	16.000	0.476
thigh (ea)	7.5	7.024	8.353	7.5	7.024	8.353	40.0	39.048	32.000	0.476
leg (ea)	6.0	5.524	6.671	6.0	5.524	6.671	40.0	39.048	32.000	0.476
arm (ea)	5.0	4.524	5.544	5.0	4.524	5.544	60.0	59.048	48.000	0.476

Referring to Fig. 3, the relationship of the additional parameters listed above (e.g., a, a', and b', etc.) is straightforward. Therefore, these parameters are not listed in the remaining tables of Appendix A.

% difference in height = -10%

bottle	a*	b*	z*	t
head	10.015	7.372	18.000	0.476
neck	6.863	6.863	9.000	0.476
thorax	10.529	15.806	36.000	0.476
pelvis	10.543	18.999	18.000	0.476
thigh (ea)	7.890	7.890	36.000	0.476
leg (ea)	6.307	6.307	36.000	0.476
arm (ea)	5.249	5.249	54.000	0.476

% difference in height = -5%

bottle	a*	b*	z*	t
head	9.747	7.178	19.000	0.476
neck	6.674	6.674	9.500	0.476
thorax	10.254	15.387	38.000	0.476
pelvis	10.260	18.479	19.000	0.476
thigh (ea)	7.687	7.687	38.000	0.476
leg (ea)	6.147	6.147	38.000	0.476
arm (ea)	5.119	5.119	57.000	0.476

All distances are reported in cm. Unless otherwise specified, t = t*.

Experiment #1 (cont.)
Vary the height of the phantom.

% difference in height = 5%

bottle	a*	b*	z*	t
head	9.272	6.835	21.000	0.476
neck	6.340	6.340	10.500	0.476
thorax	9.765	14.642	42.000	0.476
pelvis	9.759	17.557	21.000	0.476
thigh (ea)	7.327	7.327	42.000	0.476
leg (ea)	5.864	5.864	42.000	0.476
arm (ea)	4.889	4.889	63.000	0.476

% difference in height = 10%

bottle	a*	b*	z*	t
head	9.061	6.682	22.000	0.476
neck	6.192	6.192	11.000	0.476
thorax	9.547	14.309	44.000	0.476
pelvis	9.536	17.147	22.000	0.476
thigh (ea)	7.166	7.166	44.000	0.476
leg (ea)	5.737	5.737	44.000	0.476
arm (ea)	4.786	4.786	66.000	0.476

% difference in height = 20%

bottle	a*	b*	z*	t
head	8.680	6.407	24.000	0.476
neck	5.928	5.928	12.000	0.476
thorax	9.153	13.708	48.000	0.476
pelvis	9.134	16.407	24.000	0.476
thigh (ea)	6.875	6.875	48.000	0.476
leg (ea)	5.508	5.508	48.000	0.476
arm (ea)	4.600	4.600	72.000	0.476

Experiment #2A
Vary the fill volume of the phantom; hold the height constant.

% difference in fill volume = -20%

bottle	a*	b*	z*	t
head	8.547	6.311	20.000	0.476
neck	5.864	5.864	10.000	0.476
thorax	8.995	13.467	40.000	0.476
pelvis	8.995	16.150	20.000	0.476
thigh (ea)	6.758	6.758	40.000	0.476
leg (ea)	5.417	5.417	40.000	0.476
arm (ea)	4.522	4.522	60.000	0.476

% difference in fill volume = -10%

bottle	a*	b*	z*	t
head	9.037	6.665	20.000	0.476
neck	6.191	6.191	10.000	0.476
thorax	9.511	14.255	40.000	0.476
pelvis	9.511	17.101	20.000	0.476
thigh (ea)	7.140	7.140	40.000	0.476
leg (ea)	5.717	5.717	40.000	0.476
arm (ea)	4.768	4.768	60.000	0.476

% difference in fill volume = -5%

bottle	a*	b*	z*	t
head	9.272	6.835	20.000	0.476
neck	6.347	6.347	10.000	0.476
thorax	9.759	14.632	40.000	0.476
pelvis	9.759	17.556	20.000	0.476
thigh (ea)	7.322	7.322	40.000	0.476
leg (ea)	5.860	5.860	40.000	0.476
arm (ea)	4.885	4.885	60.000	0.476

All distances are reported in cm. Unless otherwise specified, t = t*.

Experiment #2A (cont.)
Vary the fill volume of the phantom; hold the height constant.

% difference in fill volume = 5%

bottle	a*	b*	z*	t
head	9.723	7.161	20.000	0.476
neck	6.649	6.649	10.000	0.476
thorax	10.235	15.359	40.000	0.476
pelvis	10.235	18.433	20.000	0.476
thigh (ea)	7.673	7.673	40.000	0.476
leg (ea)	6.136	6.136	40.000	0.476
arm (ea)	5.112	5.112	60.000	0.476

% difference in fil' volume = 10%

bottle	a*	b*	z*	t
head	9.940	7.318	20.000	0.476
neck	6.794	6.794	10.000	0.476
thorax	10.465	15.709	40.000	0.476
pelvis	10.465	18.855	20.000	0.476
thigh (ea)	7.843	7.843	40.000	0.476
leg (ea)	6.270	6.270	40.000	0.476
arm (ea)	5.221	5.221	60.000	0.476

% difference in fill volume = 20%

bottle	a*	b*	z*	t
head	10.361	7.623	20.000	0.476
neck	7.075	7.075	10.000	0.476
thorax	10.909	16.386	40.000	0.476
pelvis	10.909	19.673	20.000	0.476
thigh (ea)	8.170	8.170	40.000	0.476
leg (ea)	6.527	6.527	40.000	0.476
arm (ea)	5.432	5.432	60.000	0.476

Experiment #2B
Vary the fill volume of the phantom; vary the height proportionately.

% difference in fill volume = -20%

bottle	a*	b*	z*	t
head	8.853	6.532	18.635	0.476
neck	6.068	6.068	9.351	0.476
thorax	9.317	13.959	37.201	0.476
pelvis	9.317	16.744	18.635	0.476
thigh (ea)	6.997	6.997	37.201	0.476
leg (ea)	5.604	5.604	37.201	0.476
arm (ea)	4.676	4.676	55.767	0.476

% difference in fill volume = -10%

bottle	a*	b*	z*	t
head	9.189	6.775	19.343	0.476
neck	6.292	6.292	9.688	0.476
thorax	9.671	14.499	38.652	0.476
pelvis	9.671	17.395	19.343	0.476
thigh (ea)	7.258	7.258	38.652	0.476
leg (ea)	5.809	5.809	38.652	0.476
arm (ea)	4.844	4.844	57.962	0.476

% difference in fill volume = -5%

bottle	a*	b*	z*	t
head	9.347	6.889	19.677	0.476
neck	6.398	6.398	9.847	0.476
thorax	9.839	14.754	39.338	0.476
pelvis	9.839	17.703	19.677	0.476
thigh (ea)	7.381	7.381	39.338	0.476
leg (ea)	5.906	5.906	39.338	0.476
arm (ea)	4.923	4.923	58.999	0.476

All distances are reported in cm. Unless otherwise specified, $t = t^*$.

Experiment #2B (cont.)
Vary the fill volume of the phantom; vary the height proportionately.

% difference in fill volume = 5%

bottle	a*	b*	z*	t
head	9.648	7.107	20.312	0.476
neck	6.599	6.599	10.148	0.476
thorax	10.156	15.238	40.640	0.476
pelvis	10.156	18.287	20.312	0.476
thigh (ea)	7.615	7.615	40.640	0.476
leg (ea)	6.091	6.091	40.640	0.476
arm (ea)	5.074	5.074	60.968	0.476

% difference in fill volume = 10%

bottle	a*	b*	z*	t
head	9.791	7.211	20.615	0.476
neck	6.694	6.694	10.292	0.476
thorax	10.307	15.469	41.260	0.476
pelvis	10.307	18.566	20.615	0.476
thigh (ea)	7.727	7.727	41.260	0.476
leg (ea)	6.178	6.178	41.260	0.476
arm (ea)	5.146	5.146	61.906	0.476

% difference in fill volume = 20%

bottle	a*	b*	z*	t
head	10.065	7.409	21.194	0.476
neck	6.877	6.877	10.567	0.476
thorax	10.597	15.910	42.447	0.476
pelvis	10.597	19.098	21.194	0.476
thigh (ea)	7.940	7.940	42.447	0.476
leg (ea)	6.346	6.346	42.447	0.476
arm (ea)	5.283	5.283	63.700	0.476

Experiment #3A
Vary the density of the polyurethane fill material.

BOMAB phantom dimensions are those given in Table 1 for the average adult male human body.

% difference in density of polyurethane fill material	μ/ρ ($cm^2\ g^{-1}$)
0% (standard density)	1.09
-20%	0.87
-10%	0.98
-5%	1.04
5%	1.14
10%	1.12
20%	1.31

Experiment #3B
Vary the density of the water fill material.

BOMAB phantom dimensions are those given in Table 1 for the average adult male human body.

% difference in density of water fill material	μ/ρ ($cm^2\ g^{-1}$)
0% (standard density)	1.00
-20%	0.80
-10%	0.90
-5%	0.95
5%	1.05
10%	1.10
20%	1.20

Experiment #4
Vary the wall thickness of the phantom.

% difference in wall thickness = -20%

bottle	a*	b*	z*	t	t*
head	9.405	6.905	19.810	0.476	0.381
neck	6.405	6.405	9.810	0.476	0.381
thorax	9.905	14.905	39.810	0.476	0.381
pelvis	9.905	17.905	19.810	0.476	0.381
thigh (ea)	7.405	7.405	39.810	0.476	0.381
leg (ea)	5.905	5.905	39.810	0.476	0.381
arm (ea)	4.905	4.905	59.810	0.476	0.381

% difference in wall thickness = -10%

bottle	a*	b*	z*	t	t*
head	9.452	6.952	19.905	0.476	0.428
neck	6.452	6.452	9.905	0.476	0.428
thorax	9.952	14.952	39.905	0.476	0.428
pelvis	9.952	17.952	19.905	0.476	0.428
thigh (ea)	7.452	7.452	39.905	0.476	0.428
leg (ea)	5.952	5.952	39.905	0.476	0.428
arm (ea)	4.952	4.952	59.905	0.476	0.428

% difference in wall thickness = -5%

bottle	a*	b*	z*	t	t*
head	9.476	6.976	19.952	0.476	0.452
neck	6.476	6.476	9.952	0.476	0.452
thorax	9.976	14.976	39.952	0.476	0.452
pelvis	9.976	17.976	19.952	0.476	0.452
thigh (ea)	7.476	7.476	39.952	0.476	0.452
leg (ea)	5.976	5.976	39.952	0.476	0.452
arm (ea)	4.976	4.976	59.952	0.476	0.452

All distances are reported in cm.

Experiment #4 (cont.)
Vary the wall thickness of the phantom.

% difference in wall thickness = 5%

bottle	a*	b*	z*	t	t*
head	9.524	7.024	20.048	0.476	0.500
neck	6.524	6.524	10.048	0.476	0.500
thorax	10.024	15.024	40.048	0.476	0.500
pelvis	10.024	18.024	20.048	0.476	0.500
thigh (ea)	7.524	7.524	40.048	0.476	0.500
leg (ea)	6.024	6.024	40.048	0.476	0.500
arm (ea)	5.024	5.024	60.048	0.476	0.500

% difference in wall thickness = 10%

bottle	a*	b*	z*	t	t*
head	9.548	7.048	20.095	0.476	0.524
neck	6.548	6.548	10.095	0.476	0.524
thorax	10.048	15.048	40.095	0.476	0.524
pelvis	10.048	18.048	20.095	0.476	0.524
thigh (ea)	7.548	7.548	40.095	0.476	0.524
leg (ea)	6.048	6.048	40.095	0.476	0.524
arm (ea)	5.048	5.048	60.095	0.476	0.524

% difference in wall thickness = 20%

bottle	a*	b*	z*	t	t*
head	9.595	7.095	20.190	0.476	0.571
neck	6.595	6.595	10.190	0.476	0.571
thorax	10.095	15.095	40.190	0.476	0.571
pelvis	10.095	18.095	20.190	0.476	0.571
thigh (ea)	7.595	7.595	40.190	0.476	0.571
leg (ea)	6.095	6.095	40.190	0.476	0.571
arm (ea)	5.095	5.095	60.190	0.476	0.571

Experiment #4 (cont.)
Vary the wall thickness of the phantom.

Wall thickness is defined as 10 mm.

bottle	a*	b*	z*	t	t*
head	10.024	7.524	21.048	0.476	1.000
neck	7.024	7.024	11.048	0.476	1.000
thorax	10.524	15.524	41.048	0.476	1.000
pelvis	10.524	18.524	21.048	0.476	1.000
thigh (ea)	8.024	8.024	41.048	0.476	1.000
leg (ea)	6.524	6.524	41.048	0.476	1.000
arm (ea)	5.524	5.524	61.048	0.476	1.000

Experiment #5A
Vary the source concentration of the thorax.

BOMAB phantom dimensions are those given in Table 1 for the average adult male human body.

% difference in source concentration of polyurethane fill material within the thorax	Normalized source photon concentration (source photons cm^{-3})
0% (standard concentration throughout phantom)	1.00
-20%	0.80
-10%	0.90
-5%	0.95
5%	1.05
10%	1.10
20%	1.20

Experiment #5B
Vary the source concentration of the pelvis.

BOMAB phantom dimensions are those given in Table 1 for the average adult male human body.

% difference in source concentration of polyurethane fill material within the pelvis	Normalized source photon concentration (source photons cm^{-3})
0% (standard concentration throughout phantom)	1.00
-20%	0.80
-10%	0.90
-5%	0.95
5%	1.05
10%	1.10
20%	1.20

Experiment #5C
Vary the source concentration of the thorax, pelvis, and arms.

BOMAB phantom dimensions are those given in Table 1 for the average adult male human body.

% difference in source concentration of polyurethane fill material within the thorax pelvis, and arms	Normalized source photon concentration (source photons cm^{-3})
0% (standard concentration throughout phantom)	1.00
-20%	0.80
-10%	0.90
-5%	0.95
5%	1.05
10%	1.10
20%	1.20

APPENDIX B. RESULTS IN TABULAR FORM

Experiment #1
Vary the height of the phantom.

Relative BOMAB surface current
(source energy photons/source photon)

% change	0.200 MeV	3σ	0.662 MeV	3σ	1.460 MeV	3σ
-20%	0.331710	0.004478	0.453070	0.004757	0.557120	0.004680
-10%	0.342120	0.004516	0.464040	0.004733	0.567740	0.004769
-5%	0.347160	0.004478	0.469450	0.004788	0.572730	0.004639
0%	0.352097	0.001479	0.473819	0.001564	0.577123	0.001558
5%	0.357260	0.004501	0.479270	0.004745	0.582470	0.004718
10%	0.361840	0.004559	0.484300	0.004795	0.587490	0.004582
20%	0.370410	0.004556	0.493160	0.004734	0.596460	0.004652

Relative PNL in vivo system detector current
(source energy photons incident upon detectors/source photon)

% change	0.200 MeV	3σ	0.662 MeV	3σ	1.460 MeV	3σ
-20%	0.043379	0.000612	0.060375	0.000706	0.075330	0.000791
-10%	0.047599	0.000643	0.065636	0.000748	0.081459	0.000831
-5%	0.047973	0.000648	0.065900	0.000751	0.081506	0.000831
0%	0.048046	0.000202	0.065956	0.000237	0.081499	0.000269
5%	0.048361	0.000638	0.066000	0.000752	0.081492	0.000831
10%	0.048355	0.000638	0.065939	0.000752	0.081114	0.000827
20%	0.046934	0.000634	0.063681	0.000726	0.077889	0.000794

Relative PNL 29-cm NaI detector current
(source energy photons incident upon 29-cm NaI detector/source photon)

% change	0.200 MeV	3σ	0.662 MeV	3σ	1.460 MeV	3σ
-20%	0.013213	0.000341	0.018628	0.000408	0.023501	0.000451
-10%	0.016134	0.000378	0.022721	0.000450	0.028653	0.000499
-5%	0.016549	0.000382	0.023253	0.000453	0.029302	0.000510
0%	0.016479	0.000119	0.023265	0.000140	0.029343	0.000158
5%	0.016490	0.000381	0.023082	0.000450	0.029140	0.000507
10%	0.016247	0.000380	0.022818	0.000445	0.028652	0.000499
20%	0.015639	0.000371	0.021919	0.000441	0.027361	0.000492

Experiment #2A
Vary the fill volume of the phantom; hold the height constant.

Relative BOMAB surface current
(source energy photons/source photon)

% change	0.200 MeV	3σ	0.662 MeV	3σ	1.460 MeV	3σ
-20%	0.377040	0.004638	0.500300	0.004803	0.602480	0.004699
-10%	0.364050	0.004587	0.486730	0.004673	0.589490	0.004598
-5%	0.358170	0.004513	0.480170	0.004754	0.583740	0.004728
0%	0.352097	0.001479	0.473819	0.001564	0.577123	0.001558
5%	0.346710	0.004473	0.468980	0.004784	0.572360	0.004636
10%	0.341580	0.004509	0.463450	0.004727	0.566920	0.004762
20%	0.332540	0.004489	0.453400	0.004761	0.556990	0.004679

Relative PNL in vivo system detector current
(source energy photons incident upon detectors/source photon)

% change	0.200 MeV	3σ	0.662 MeV	3σ	1.460 MeV	3σ
-20%	0.056127	0.000690	0.075879	0.000797	0.092436	0.000860
-10%	0.051804	0.000668	0.070558	0.000762	0.086577	0.000831
-5%	0.049872	0.000658	0.068108	0.000756	0.083960	0.000831
0%	0.048046	0.000202	0.065956	0.000237	0.081499	0.000269
5%	0.046442	0.000627	0.063876	0.000728	0.079186	0.000808
10%	0.044933	0.000620	0.062017	0.000726	0.077133	0.000810
20%	0.042106	0.000606	0.058559	0.000703	0.073180	0.000790

Relative PNL 29-cm NaI detector current
(source energy photons incident upon 29-cm NaI detector/source photon)

% change	0.200 MeV	3σ	0.662 MeV	3σ	1.460 MeV	3σ
-20%	0.019359	0.000412	0.026880	0.000484	0.033354	0.000540
-10%	0.017857	0.000396	0.024956	0.000472	0.031238	0.000525
-5%	0.017178	0.000392	0.024086	0.000462	0.030290	0.000518
0%	0.016479	0.000119	0.023265	0.000140	0.029343	0.000158
5%	0.015961	0.000378	0.022572	0.000447	0.028488	0.000496
10%	0.015430	0.000370	0.021902	0.000440	0.027754	0.000491
20%	0.014417	0.000359	0.020644	0.000427	0.026310	0.000481

Experiment #2B
Vary the fill volume of the phantom; vary the height proportionately.

Relative BOMAB surface current
(source energy photons/source photon)

% change	0.200 MeV	3σ	0.662 MeV	3σ	1.460 MeV	3σ
-20%	0.369420	0.004544	0.492540	0.004728	0.595670	0.004646
-10%	0.360530	0.004543	0.482970	0.004781	0.586400	0.004750
-5%	0.356210	0.004595	0.478590	0.004738	0.581810	0.004713
0%	0.352097	0.001479	0.473819	0.001564	0.577123	0.001558
5%	0.348170	0.004491	0.470490	0.004799	0.574100	0.004650
10%	0.344580	0.004548	0.466560	0.004759	0.570460	0.004621
20%	0.337880	0.004460	0.458930	0.004681	0.562780	0.004727

Relative PNL in vivo system detector current
(source energy photons incident upon detectors/source photon)

% change	0.200 MeV	3σ	0.662 MeV	3σ	1.460 MeV	3σ
-20%	0.056031	0.000689	0.075831	0.000796	0.092626	0.000861
-10%	0.051614	0.000666	0.070407	0.000760	0.086470	0.000856
-5%	0.049755	0.000657	0.068012	0.000755	0.083811	0.000830
0%	0.048046	0.000202	0.065956	0.000237	0.081499	0.000269
5%	0.046558	0.000629	0.063933	0.000729	0.079211	0.000808
10%	0.045147	0.000623	0.062197	0.000728	0.077182	0.000810
20%	0.042299	0.000609	0.058571	0.000703	0.073020	0.000789

Relative PNL 29-cm NaI detector current
(source energy photons incident upon 29-cm NaI detector/source photon)

% change	0.200 MeV	3σ	0.662 MeV	3σ	1.460 MeV	3σ
-20%	0.019270	0.000410	0.026730	0.000481	0.033237	0.000538
-10%	0.017894	0.000397	0.025033	0.000466	0.031294	0.000526
-5%	0.017158	0.000391	0.024102	0.000463	0.030280	0.000518
0%	0.016479	0.000119	0.023265	0.000140	0.029343	0.000158
5%	0.015917	0.000377	0.022460	0.000445	0.028415	0.000494
10%	0.015389	0.000369	0.021794	0.000438	0.027625	0.000489
20%	0.014267	0.000355	0.020366	0.000422	0.025969	0.000475

Experiment #3A
Vary the density of the polyurethane fill material.

Relative BOMAB surface current
(source energy photons/source photon)

% change	0.200 MeV	3σ	0.662 MeV	3σ	1.460 MeV	3σ
-20%	0.405090	0.004618	0.528440	0.004756	0.629370	0.004531
-10%	0.376490	0.004631	0.500570	0.004805	0.602410	0.004699
-5%	0.363250	0.004577	0.485740	0.004809	0.589150	0.004595
0%	0.352097	0.001479	0.473819	0.001564	0.577123	0.001558
5%	0.341730	0.004511	0.463510	0.004728	0.567010	0.004763
10%	0.330300	0.004459	0.450760	0.004733	0.554580	0.004658
20%	0.310270	0.004375	0.428800	0.004631	0.533150	0.004798

Relative PNL in vivo system detector current
(source energy photons incident upon detectors/source photon)

% change	0.200 MeV	3σ	0.662 MeV	3σ	1.460 MeV	3σ
-20%	0.055749	0.000686	0.074046	0.000777	0.089187	0.000856
-10%	0.051629	0.000666	0.069800	0.000775	0.085217	0.000844
-5%	0.049595	0.000655	0.067616	0.000751	0.083090	0.000823
0%	0.048046	0.000202	0.065956	0.000237	0.081499	0.000269
5%	0.046614	0.000629	0.064300	0.000733	0.079872	0.000815
10%	0.044918	0.000620	0.062452	0.000731	0.078076	0.000796
20%	0.042027	0.000605	0.059345	0.000712	0.074852	0.000786

Relative PNL 29-cm NaI detector current
(source energy photons incident upon 29-cm NaI detector/source photon)

% change	0.200 MeV	3σ	0.662 MeV	3σ	1.460 MeV	3σ
-20%	0.019360	0.000412	0.026474	0.000484	0.032446	0.000535
-10%	0.017834	0.000396	0.024852	0.000470	0.030894	0.000519
-5%	0.017120	0.000390	0.023997	0.000461	0.030035	0.000514
0%	0.016479	0.000119	0.023265	0.000140	0.029343	0.000158
5%	0.015996	0.000374	0.022718	0.000450	0.028789	0.000501
10%	0.015388	0.000369	0.022026	0.000443	0.028086	0.000497
20%	0.014343	0.000357	0.020814	0.000431	0.026841	0.000483

Experiment #3B
Vary the density of the water fill material.

Relative BOMAB surface current
(source energy photons/source photon)

% change	0.200 MeV	3σ	0.662 MeV	3σ	1.460 MeV	3σ
-20%	0.419610	0.004658	0.543230	0.004726	0.642230	0.004624
-10%	0.391710	0.004583	0.515570	0.004795	0.616890	0.004627
-5%	0.378870	0.004546	0.502640	0.004675	0.604540	0.004715
0%	0.366925	0.001431	0.489404	0.001468	0.591796	0.001420
5%	0.355840	0.004590	0.478030	0.004732	0.581210	0.004708
10%	0.344910	0.004553	0.466760	0.004761	0.570690	0.004623
20%	0.325410	0.004491	0.445610	0.004679	0.549440	0.004780

Relative PNL in vivo system detector current
(source energy photons incident upon detectors/source photon)

% change	0.200 MeV	3σ	0.662 MeV	3σ	1.460 MeV	3σ
-20%	0.057917	0.000695	0.076258	0.000801	0.091144	0.000875
-10%	0.053768	0.000677	0.072109	0.000779	0.087347	0.000839
-5%	0.051941	0.000670	0.070127	0.000757	0.085506	0.000847
0%	0.050217	0.000211	0.068282	0.000246	0.083750	0.000251
5%	0.048571	0.000641	0.066437	0.000737	0.081977	0.000812
10%	0.047052	0.000635	0.064806	0.000739	0.080355	0.000820
20%	0.044188	0.000623	0.061690	0.000722	0.077261	0.000811

Relative PNL 29-cm NaI detector current
(source energy photons incident upon 29-cm NaI detector/source photon)

% change	0.200 MeV	3σ	0.662 MeV	3σ	1.460 MeV	3σ
-20%	0.020197	0.000424	0.027326	0.000492	0.033253	0.000539
-10%	0.018613	0.000408	0.025739	0.000479	0.031720	0.000523
-5%	0.017940	0.000398	0.024992	0.000465	0.030994	0.000521
0%	0.017281	0.000124	0.024152	0.000145	0.030242	0.000163
5%	0.016734	0.000387	0.023541	0.000452	0.029600	0.000506
10%	0.016166	0.000378	0.022914	0.000447	0.028946	0.000504
20%	0.015123	0.000367	0.021728	0.000437	0.027777	0.000492

Experiment #4
Vary the wall thickness of the phantom.

Relative BOMAB surface current
(source energy photons/source photon)

% change	0.200 MeV	3σ	0.662 MeV	3σ	1.460 MeV	3σ
-20%	0.359650	0.004532	0.480910	0.004761	0.583110	0.004723
-10%	0.356110	0.004594	0.477700	0.004729	0.580520	0.004702
-5%	0.354360	0.004571	0.476250	0.004715	0.579340	0.004693
0%	0.352097	0.001479	0.473819	0.001564	0.577123	0.001558
5%	0.351120	0.004529	0.473050	0.004683	0.576540	0.004670
10%	0.349290	0.004506	0.471520	0.004668	0.575220	0.004659
20%	0.346220	0.004466	0.468450	0.004778	0.572560	0.004638
110%	0.318290	0.004392	0.443230	0.004654	0.550810	0.004792

Relative PNL in vivo system detector current
(source energy photons incident upon detectors/source photon)

% change	0.200 MeV	3σ	0.662 MeV	3σ	1.460 MeV	3σ
-20%	0.049421	0.000652	0.067249	0.000746	0.082869	0.000820
-10%	0.048781	0.000644	0.066606	0.000739	0.082211	0.000814
-5%	0.048429	0.000639	0.066214	0.000755	0.081836	0.000810
0%	0.048046	0.000202	0.065956	0.000237	0.081499	0.000269
5%	0.047766	0.000645	0.065555	0.000747	0.081141	0.000828
10%	0.047413	0.000640	0.065203	0.000743	0.080785	0.000824
20%	0.046788	0.000632	0.064493	0.000735	0.080125	0.000817
110%	0.041503	0.000598	0.058934	0.000707	0.074353	0.000781

Relative PNL 29-cm NaI detector current
(source energy photons incident upon 29-cm NaI detector/source photon)

% change	0.200 MeV	3σ	0.662 MeV	3σ	1.460 MeV	3σ
-20%	0.017006	0.000388	0.023777	0.000457	0.029864	0.000511
-10%	0.016801	0.000383	0.023575	0.000453	0.029642	0.000507
-5%	0.016672	0.000385	0.023441	0.000457	0.029479	0.000504
0%	0.016479	0.000119	0.023265	0.000140	0.029343	0.000158
5%	0.016436	0.000380	0.023204	0.000452	0.029253	0.000509
10%	0.016294	0.000381	0.023060	0.000450	0.029128	0.000507
20%	0.016093	0.000377	0.022775	0.000451	0.028828	0.000502
110%	0.014144	0.000352	0.020596	0.000426	0.026510	0.000485

Experiment #5A
Vary the source concentration of the thorax.

Relative BOMAB surface current
(source energy photons/source photon)

% change	0.200 MeV	3σ	0.662 MeV	3σ	1.460 MeV	3σ
-20%	0.357380	0.004503	0.480200	0.004754	0.583000	0.004722
-10%	0.355030	0.004580	0.477580	0.004728	0.580570	0.004703
-5%	0.353830	0.004564	0.476130	0.004714	0.579420	0.004693
0%	0.352097	0.001479	0.473819	0.001564	0.577123	0.001558
5%	0.351340	0.004532	0.473270	0.004685	0.576320	0.004668
10%	0.350090	0.004516	0.472220	0.004675	0.575110	0.004658
20%	0.348150	0.004491	0.470250	0.004797	0.573220	0.004643

Relative PNL in vivo system detector current
(source energy photons incident upon detectors/source photon)

% change	0.200 MeV	3σ	0.662 MeV	3σ	1.460 MeV	3σ
-20%	0.047672	0.000644	0.065265	0.000744	0.080503	0.000821
-10%	0.047914	0.000647	0.065664	0.000749	0.081031	0.000827
-5%	0.048092	0.000635	0.065909	0.000751	0.081376	0.000830
0%	0.048046	0.000202	0.065956	0.000237	0.081499	0.000269
5%	0.048113	0.000635	0.066022	0.000753	0.081658	0.000833
10%	0.048276	0.000637	0.066311	0.000756	0.081994	0.000812
20%	0.048555	0.000641	0.066761	0.000741	0.082573	0.000817

Relative PNL 29-cm NaI detector current
(source energy photons incident upon 29-cm NaI detector/source photon)

% change	0.200 MeV	3σ	0.662 MeV	3σ	1.460 MeV	3σ
-20%	0.015361	0.000369	0.021679	0.000436	0.027329	0.000492
-10%	0.015993	0.000374	0.022548	0.000446	0.028380	0.000502
-5%	0.016321	0.000382	0.022996	0.000448	0.028934	0.000503
0%	0.016479	0.000119	0.023265	0.000140	0.029343	0.000158
5%	0.016828	0.000384	0.023718	0.000455	0.029863	0.000511
10%	0.017109	0.000390	0.024144	0.000464	0.030365	0.000519
20%	0.017655	0.000397	0.024909	0.000471	0.031346	0.000527

Experiment #5B
Vary the source concentration of the pelvis.

Relative BOMAB surface current
(source energy photons/source photon)

% change	0.200 MeV	3σ	0.662 MeV	3σ	1.460 MeV	3σ
-20%	0.355090	0.004581	0.477550	0.004728	0.580600	0.004703
-10%	0.353930	0.004566	0.476060	0.004713	0.579200	0.004692
-5%	0.353270	0.004557	0.475420	0.004707	0.578660	0.004687
0%	0.352097	0.001479	0.473819	0.001564	0.577123	0.001558
5%	0.351860	0.004539	0.473870	0.004691	0.577200	0.004675
10%	0.351200	0.004530	0.473270	0.004685	0.576520	0.004670
20%	0.349970	0.004515	0.472160	0.004674	0.575130	0.004659

Relative PNL in vivo system detector current
(source energy photons incident upon detectors/source photon)

% change	0.200 MeV	3σ	0.662 MeV	3σ	1.460 MeV	3σ
-20%	0.048100	0.000635	0.065894	0.000751	0.081321	0.000829
-10%	0.048164	0.000636	0.065995	0.000752	0.081490	0.000831
-5%	0.048165	0.000636	0.066006	0.000752	0.081529	0.000832
0%	0.048046	0.000202	0.065956	0.000237	0.081499	0.000269
5%	0.048031	0.000648	0.065909	0.000751	0.081476	0.000831
10%	0.048047	0.000649	0.065953	0.000752	0.081554	0.000832
20%	0.048167	0.000636	0.066159	0.000754	0.081796	0.000834

Relative PNL 29-cm NaI detector current
(source energy photons incident upon 29-cm NaI detector/source photon)

% change	0.200 MeV	3σ	0.662 MeV	3σ	1.460 MeV	3σ
-20%	0.016496	0.000381	0.023209	0.000453	0.029184	0.000508
-10%	0.016539	0.000382	0.023278	0.000454	0.029282	0.000510
-5%	0.016551	0.000382	0.023312	0.000455	0.029338	0.000510
0%	0.016479	0.000119	0.023265	0.000140	0.029343	0.000158
5%	0.016566	0.000383	0.023367	0.000456	0.029415	0.000503
10%	0.016617	0.000384	0.023427	0.000457	0.029473	0.000504
20%	0.016674	0.000385	0.023532	0.000452	0.029629	0.000507

Experiment #5C
Vary the source concentration of the thorax, pelvis, and arms.

Relative BOMAB surface current
(source energy photons/source photon)

% change	0.200 MeV	3σ	0.662 MeV	3σ	1.460 MeV	3σ
-20%	0.356400	0.004491	0.479190	0.004744	0.582450	0.004718
-10%	0.354370	0.004571	0.476950	0.004722	0.580150	0.004699
-5%	0.353410	0.004559	0.475650	0.004709	0.579090	0.004691
0%	0.352097	0.001479	0.473819	0.001564	0.577123	0.001558
5%	0.351810	0.004538	0.473570	0.004688	0.576510	0.004670
10%	0.350800	0.004525	0.472760	0.004680	0.575570	0.004662
20%	0.348920	0.004501	0.471060	0.004805	0.574000	0.004649

Relative PNL in vivo system detector current
(source energy photons incident upon detectors/source photon)

% change	0.200 MeV	3σ	0.662 MeV	3σ	1.460 MeV	3σ
-20%	0.048064	0.000649	0.065761	0.000750	0.081046	0.000827
-10%	0.048156	0.000636	0.065942	0.000752	0.081393	0.000830
-5%	0.048142	0.000635	0.065947	0.000752	0.081467	0.000831
0%	0.048046	0.000202	0.065956	0.000237	0.081499	0.000269
5%	0.048081	0.000635	0.065969	0.000752	0.081570	0.000832
10%	0.048144	0.000636	0.066083	0.000753	0.081716	0.000834
20%	0.048162	0.000636	0.066198	0.000755	0.081927	0.000811

Relative PNL 29-cm NaI detector current
(source energy photons incident upon 29-cm NaI detector/source photon)

% change	0.200 MeV	3σ	0.662 MeV	3σ	1.460 MeV	3σ
-20%	0.015084	0.000367	0.021313	0.000435	0.026915	0.000484
-10%	0.015926	0.000377	0.022462	0.000445	0.028293	0.000501
-5%	0.016257	0.000380	0.022906	0.000447	0.028841	0.000502
0%	0.016479	0.000119	0.023265	0.000140	0.029343	0.000158
5%	0.016857	0.000384	0.023762	0.000456	0.029885	0.000511
10%	0.017174	0.000392	0.024170	0.000464	0.030400	0.000511
20%	0.017703	0.000393	0.024929	0.000471	0.031342	0.000527

APPENDIX C. RESULTS IN GRAPHICAL FORM

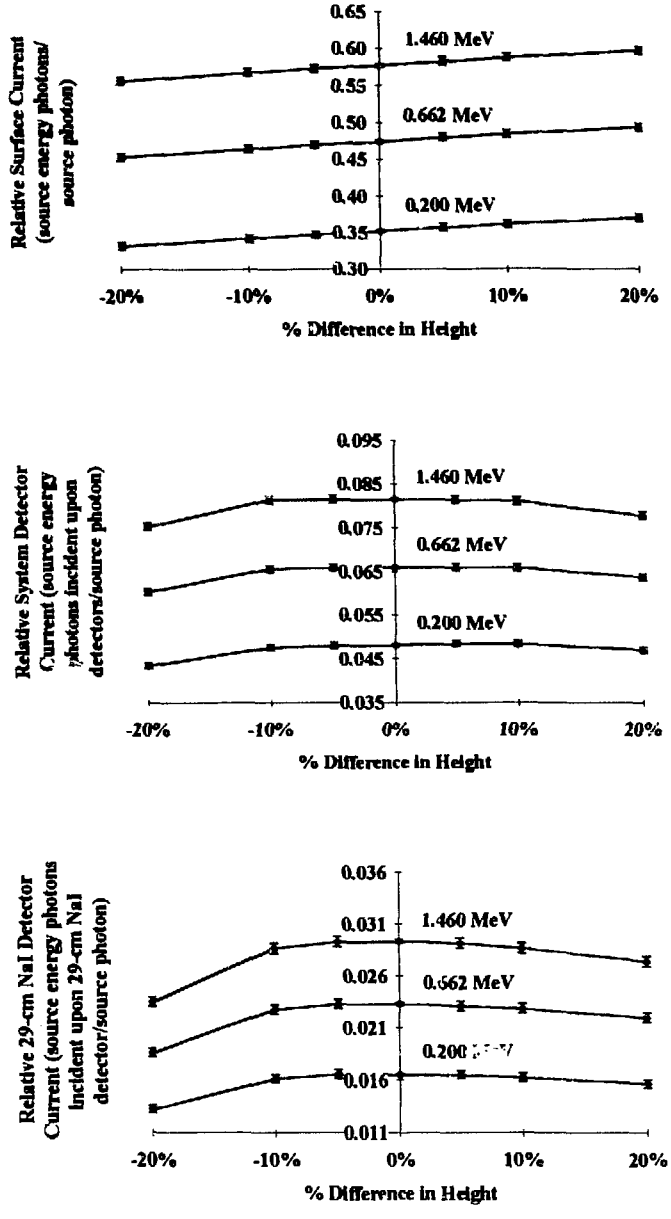

Fig. C.1. Monte Carlo results for different phantom heights (Experiment #1). Errors shown are $\pm 3\sigma$.

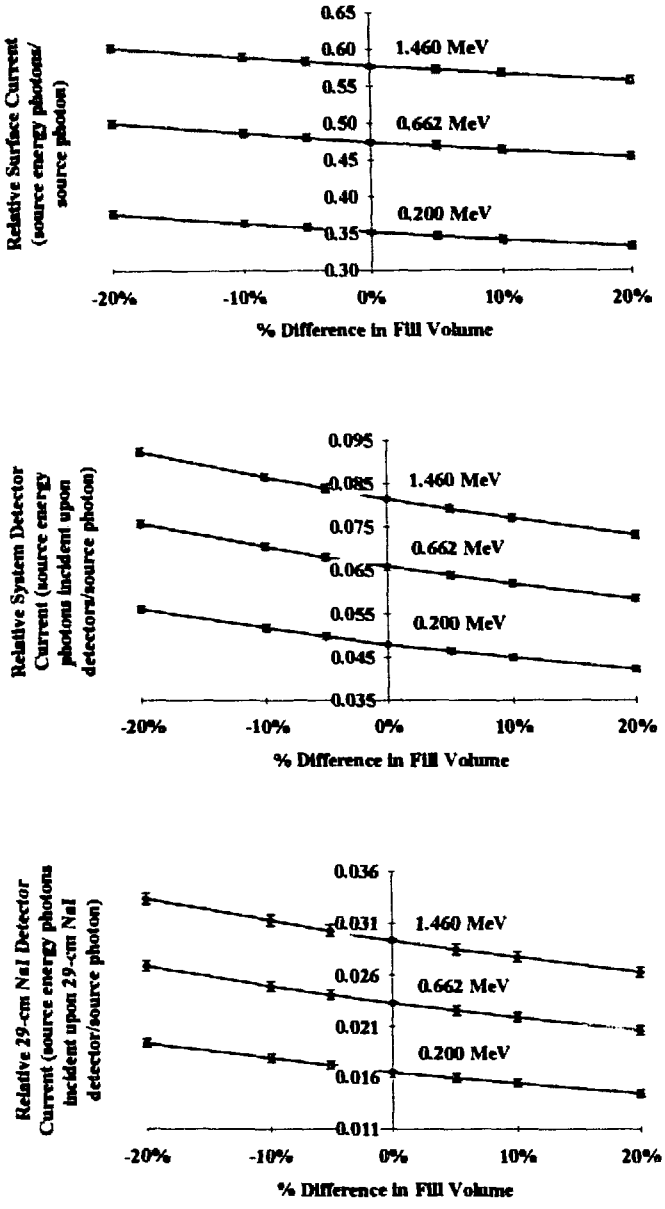

Fig. C.2. Monte Carlo results for different fill volumes of the phantom; hold the height constant (Experiment #2A). Errors shown are $\pm 3\sigma$.

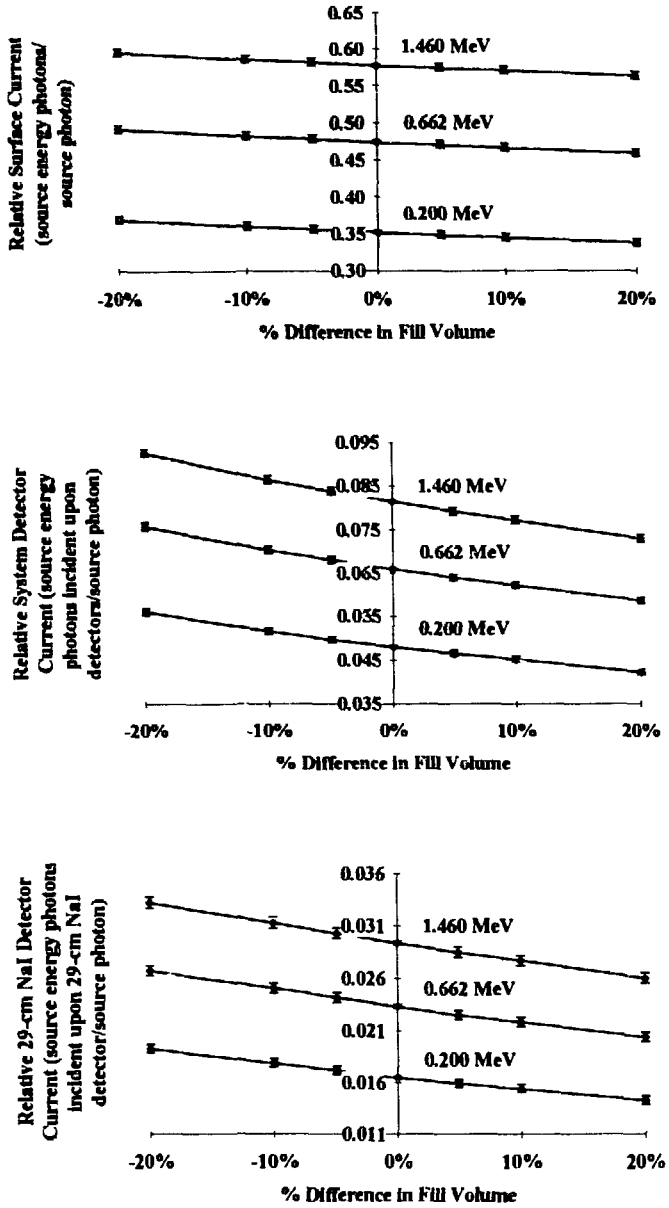

Fig. C.3. Monte Carlo results for different fill volumes of the phantom; vary the height proportionately (Experiment #2B). Errors shown are $\pm 3\sigma$.

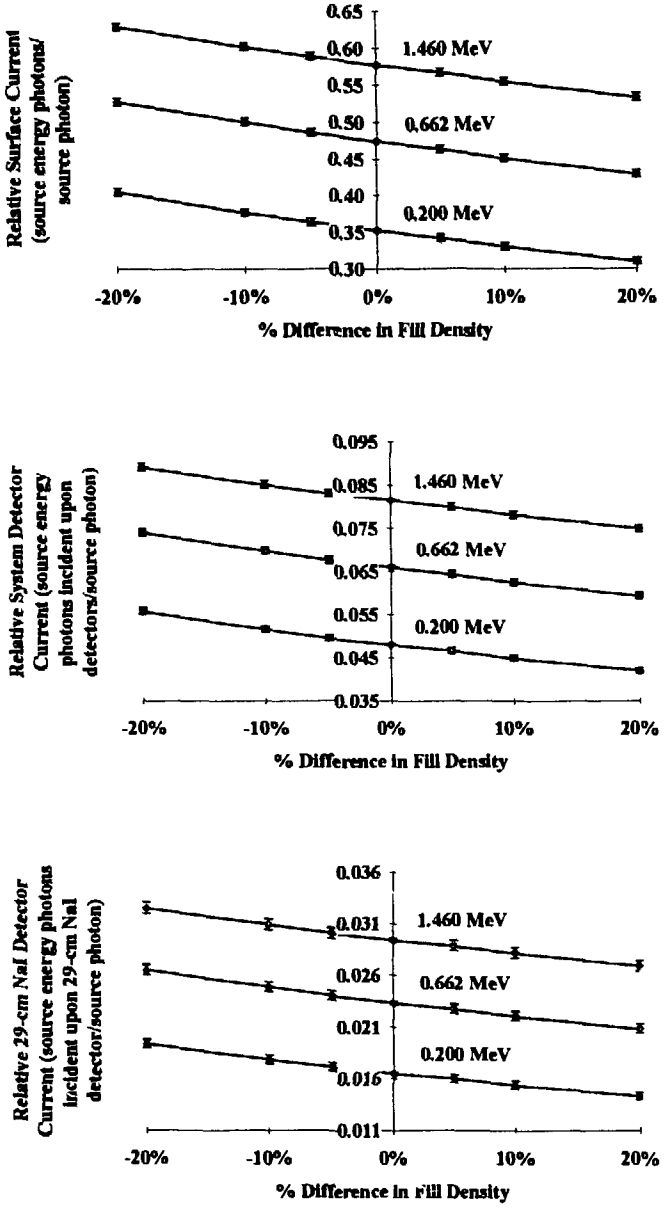

Fig. C.4. Monte Carlo results for different densities of the polyurethane fill material (Experiment #3A). Errors shown are $\pm 3\sigma$.

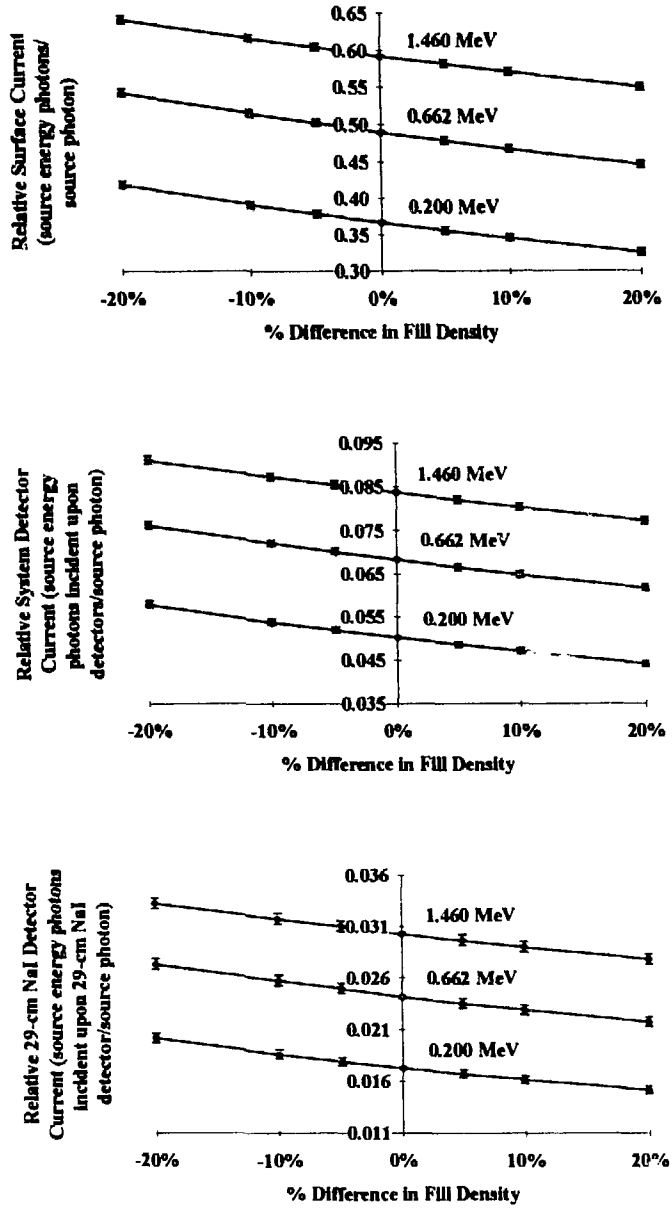

Fig. C.5. Monte Carlo results for different densities of the water fill material (Experiment #3B). Errors shown are $\pm 3\sigma$.

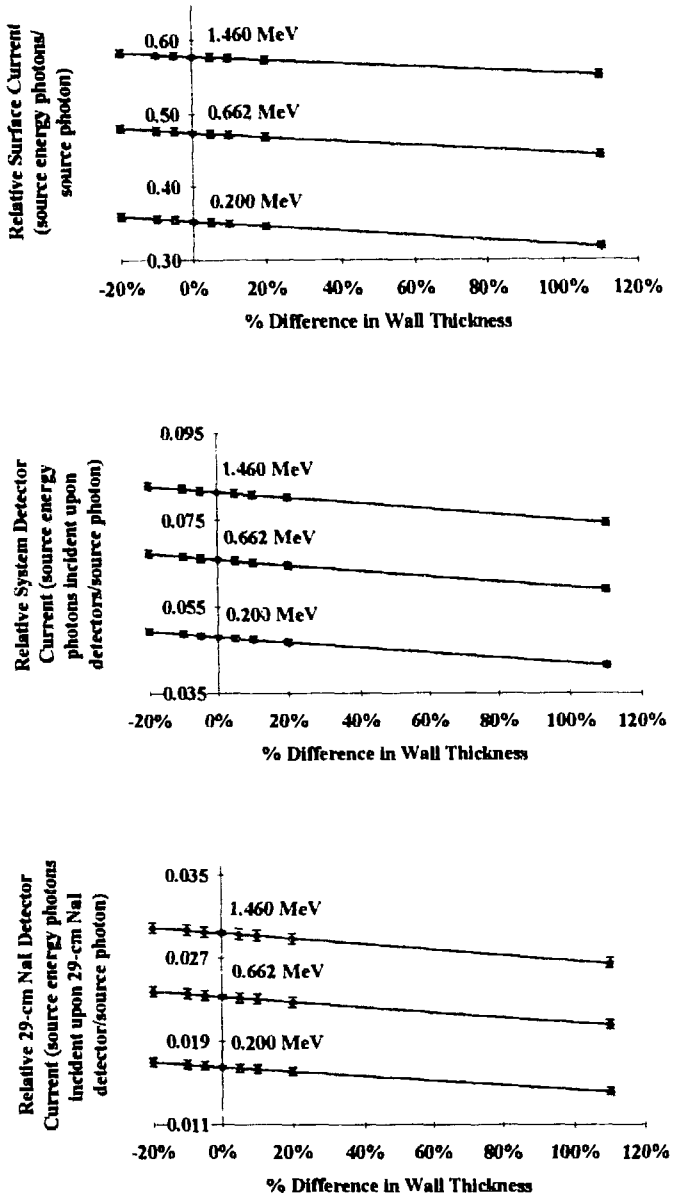

Fig. C.6. Monte Carlo results for different wall thicknesses of the phantom (Experiment #4). Errors shown are $\pm 3\sigma$.

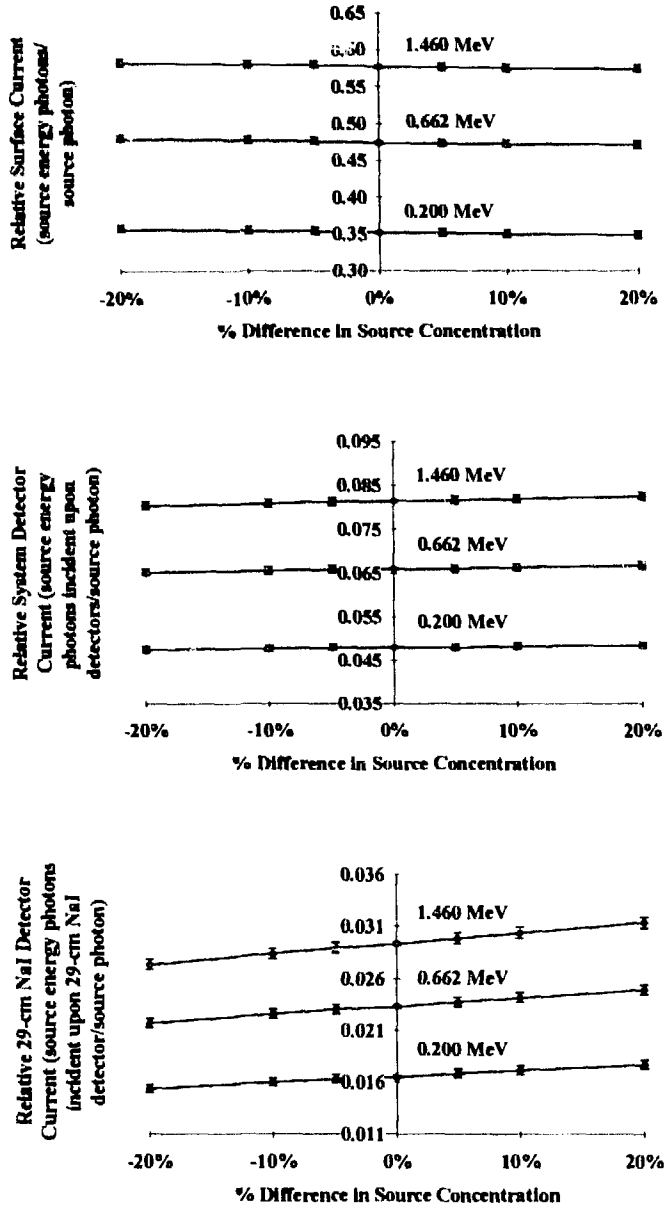

Fig. C.7. Monte Carlo results for different source concentrations of the thorax (Experiment #5A). Errors shown are $\pm 3\sigma$.

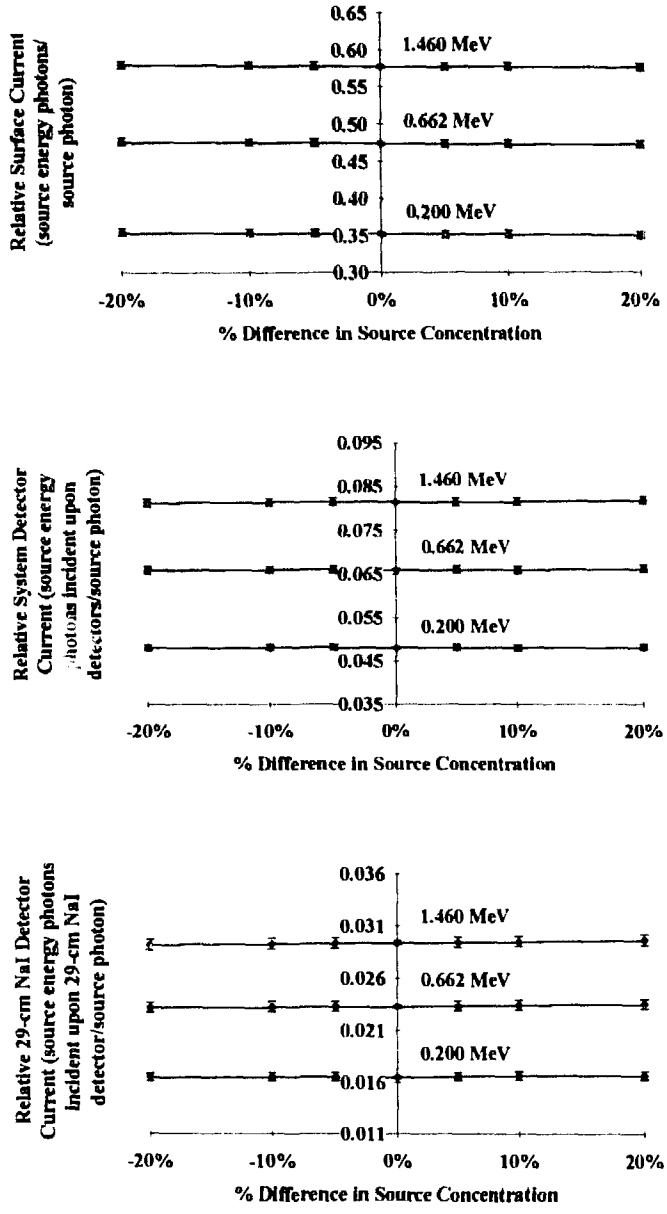

Fig. C.8. Monte Carlo results for different source concentrations of the pelvis (Experiment #5B). Errors shown are $\pm 3\sigma$.

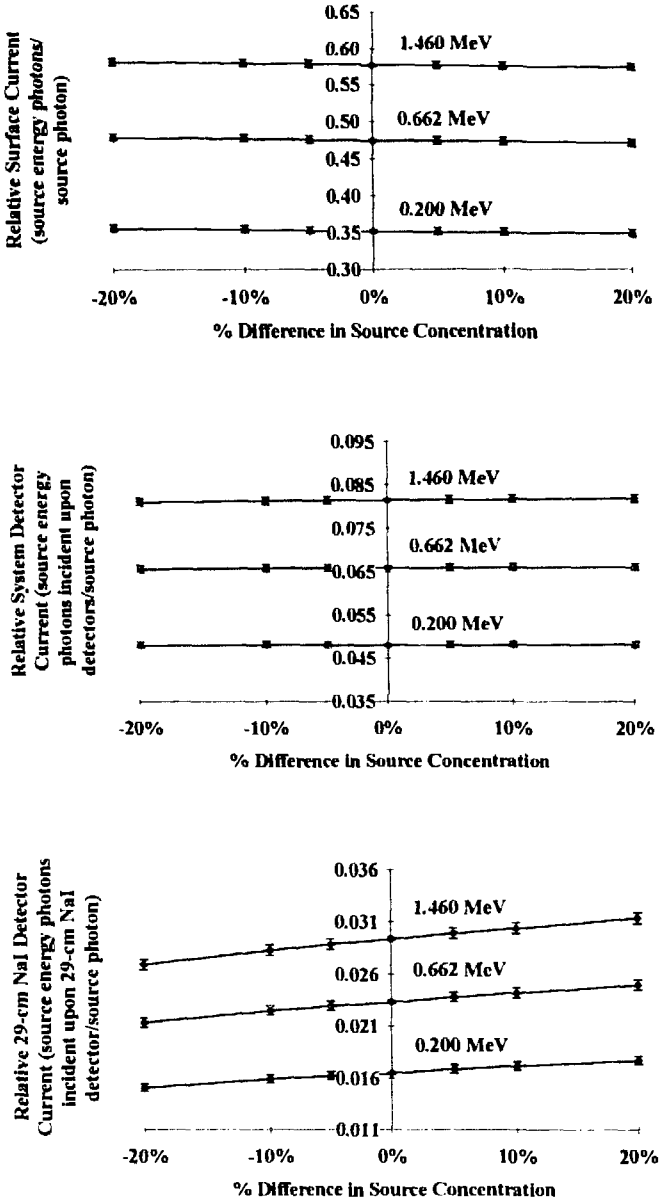

Fig. C.9. Monte Carlo results for different source concentrations of the thorax, pelvis, and arms (Experiment #5C). Errors shown are $\pm 3\sigma$.